PROCEEDINGS, 50th Workshop on Geothermal Reservoir Engineering
Stanford University, Stanford, California, February 10-12, 2025
SGP-TR-229

Enhancing Geothermal Reservoir Models with Discrete Magmatic Heat Sources

Samuel SCOTT, Guðjón Helgi EGGERTSSON, Hilmar Már EINARSSON, Andri STEFÁNSSON

Sturlugata 7, 102 Reykjavik, Iceland

samuels@hi.is

Keywords: magmatic intrusions, Krafla, high-enthalpy systems, IDDP-1, superhot geothermal, permeability

ABSTRACT

Magmatic intrusions drive fluid convection in high-enthalpy geothermal systems, yet industry-standard geothermal reservoir models represent these heat sources using fixed boundary conditions at the bottom of the model domain. This oversimplification ignores the complex heat transfer dynamics between magmatic intrusions and surrounding groundwater. This study presents the first field-scale geothermal model incorporating a discrete magmatic intrusion into the model domain, using the Krafla geothermal system in Iceland as a case study. Krafla offers unique insights with direct evidence from wells drilled into magma. The model is calibrated using the natural state temperature and fluid pressure distribution, as well as production data from the Iceland Deep Drilling Project (IDDP-1) well discharge, which encountered magma at ~2 km depth. Results indicate very high permeability near the magma chamber, which results in steep temperature gradients at the magma-hydrothermal interface and conductive heat fluxes of up to ~24 W/m². Moreover, our model shows how the large-scale thermal structure of the system, including at the depths of conventional production wells, depends on the permeability structure and heat transfer dynamics near the magma-hydrothermal interface. Despite the remaining challenges in imaging subsurface magma bodies and reconstructing complex, time-dependent magmatic histories, our findings suggest that including magmatic intrusions into reservoir models provides novel insights into the thermal structure of magma-driven geothermal systems.

1. INTRODUCTION

Groundwater can be heated to temperatures above the critical temperature of water close to magma (Heřmanská et al., 2019), as evidenced by the Iceland Deep Drilling Project well IDDP-1 in Krafla as well as numerous other wells drilled in the deeper parts of presently exploited high-temperature geothermal reservoirs (Reinsch et al., 2018). However, these supercritical/superhot "roots" are often neglected when building 3D models of exploited geothermal systems in the industry-standard TOUGH simulation codes due to temperature restrictions in the standard equation of state, EOS1 (O'Sullivan et al., 2016). More recent TOUGH models that extend to supercritical conditions (Croucher and O'Sullivan, 2008; Magnusdottir and Finsterle, 2015) still represent the supercritical roots using fixed boundary conditions on the model's bottom boundary (O'Sullivan et al., 2016; Scott et al., 2022). Thus, traditional research into magma-hydrothermal heat transfer dynamics has been siloed; petrologists and volcanologists have concentrated on magma dynamics independently of hydrothermal processes, while geothermal researchers have often oversimplified the influence of magmatic heat sources (Figure 1). Although models that explicitly simulate fluid circulation around intrusions are relatively rare (e.g., Hayba and Ingebritsen, 1997; Scott et al., 2015, 2016; Andersen and Weis, 2020), these models highlight that heat transfer processes at the magma-hydrothermal interface play a key role in controlling the thermal structure of the overlying geothermal system. Incorporating these heat transfer dynamics into geothermal and magmatic models will enhance both geothermal resource management as well as our understanding of magma's thermal evolution.

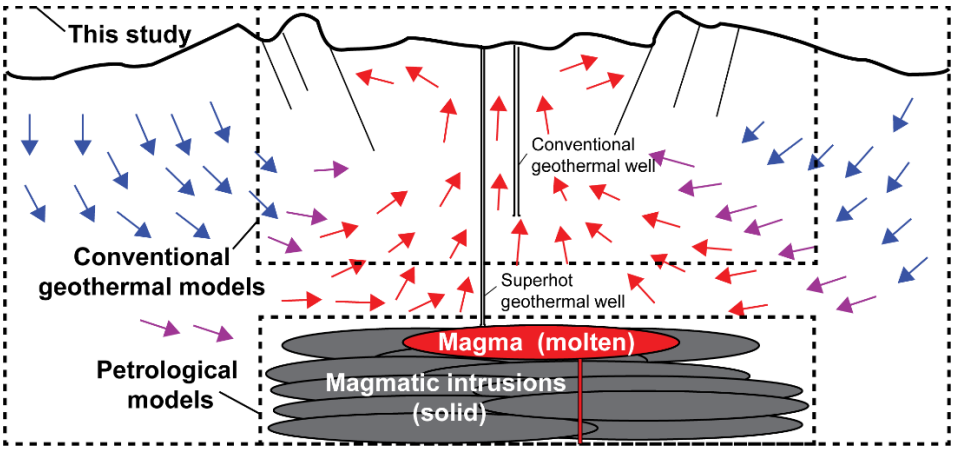

Figure 1: Conceptual framework illustrating the areas covered by petrological models, conventional geothermal models, and the integrated approach proposed in this study. Conventional geothermal wells are drilled into the shallow upflow of the geothermal system; in the future, geothermal wells may be drilled closer to the magma-hydrothermal interface.

The influence of hydrothermal circulation on the thermal evolution of magma intrusions results from an energy balance between the heat dissipated from a magma body and the heat advected away from the intrusion by flowing groundwater. Magmatic and hydrothermal domains are interconnected through heat fluxes across a boundary layer, commonly known as the 'brittle-ductile transition' (BDT), which delineates a shift from localized dilatational brittle failure to homogenous cataclastic or plastic flow (Rutter, 1986). The BDT is characterized by a permeability decrease and a shift from advection-dominated to conduction-dominated heat transfer (Hayba and Ingebritsen, 1997). This interplay is illustrated schematically in Figure 2. In high-permeability host rocks, strong fluid mass fluxes and advective heat transport in the hydrothermal system enhance heat conduction across the BDT, creating steep temperature gradients, as seen in IDDP-1, where temperatures transitioned from boiling-point-with-depth conditions to magmatic temperatures over ~50 meters (Eichelberger, 2020). Despite high rates of heat advection, fluid is heated to lower temperatures during rapid flow around the intrusion, more intensively mixed with cooler circulating waters above the intrusion, and superhot conditions are confined to the near-vicinity of the intrusion (Scott et al, 2015). Conversely, in low-permeability host rocks (Figure 2b), reduced fluid mass fluxes diminish heat advection but allow higher fluid enthalpies due to prolonged heat exchange, even as conductive heat transfer decreases. In essence, the hydrothermal system acts as a heat sink, accelerating magma cooling. However, the efficiency of this heat sink depends on factors like permeability and cold recharge availability, highlighting a need for further exploration of these dynamics.

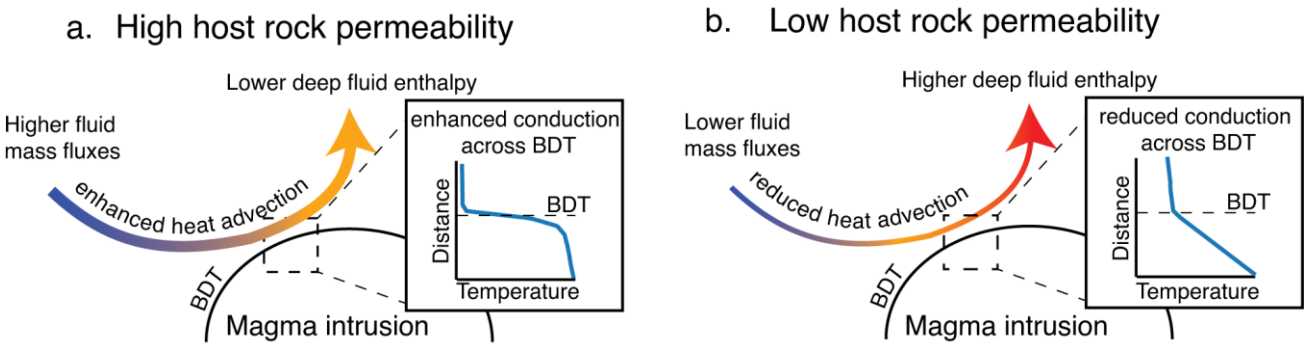

Figure 2: Schematic representation of heat transfer dynamics at the magma-hydrothermal interface for magmatic intrusions emplaced into a. high and b. low permeability host rocks.

For several decades, there has been growing interest among the geothermal industry as well as academia in the production characteristics of geothermal resources at superhot conditions (temperatures >374 °C) near magmatic intrusion (Reinsch et al., 2017). Previous studies suggested that a supercritical (temperatures >374 °C and pressures >22 MPa) well could generate up to 50 MWe (Albertsson et al., 2003; Fridleifsson et al., 2014), an order of magnitude greater than typical geothermal wells drilled in conventional high-enthalpy geothermal resources. Although superhot resources at pressures 22 MPa may have a somewhat lower potential because flow into the wells is often volumetrically constrained and the lower density of superhot water with increasing temperature results in a lower mass flow rate, this production potential is likely still considerable. The estimates of greater power generation potential are a mainly a consequence of thermodynamic considerations, including higher fluid specific enthalpy, increased fluid flow rates into the production well due to lower fluid viscosity, and the higher efficiency of power generation, rather than the characteristics (e.g. permeability conditions) of the reservoir rock close to intrusions. These thermodynamically-based estimations were supported by the drilling of the IDDP-1 well in Iceland, which tapped into a single-phase vapor resource above a shallow magmatic intrusion at 2.1 km depth (Elders et al., 2014). While short-term flow testing of this well suggested a power generation potential of up to 34 MWe (Axelsson et al., 2014; Ingason et al., 2014), damage to surface equipment forced the well to be closed prematurely, and as a result, the longer-term response of these reservoirs to production remains unclear.

Most prior modelling studies of production from superhot/supercritical reservoirs have used idealized initial and boundary conditions (Yano and Ishido, 1998; Croucher and O'Sullivan, 2008; Magnusdottir and Finsterle, 2015; Battistelli et al., 2020). For example, Battistelli et al. (2020) developed a sophisticated TOUGH2 model integrating a supercritical equation of state (EOS2H) with T2Well, a wellbore simulator, and performed coupled wellbore-reservoir flow simulations of an IDDP-1-like resource. However, these workers used a radial grid with a lateral boundary at a radius of 5 km away from the well, in order to simulate an infinite acting reservoir surrounding the well. The entire model domain was set to initial static pressure and temperature values of 15.5 MPa and 510 °C. Calibration of the model to observed mass flow rates as function of well-head pressure was obtained by using a reservoir permeability of 9.3×10^{-13} m^2. Such permeability is significantly higher than bulk permeability of most geothermal systems at >1 km depth (Manning and Ingebritsen, 1999). In contrast, Yapparova et al. (2022) used the CSMP++ platform to investigate the production characteristics of a supercritical geothermal resource above a magmatic intrusion, assuming a host rock permeability of 10^{-15} m^2, more in line with estimates of bulk permeability at >1 km depth in such systems. However, the production mass flow rates were only 3-5 kg s^{-1}, around an order of magnitude less than what was observed in IDDP-1 (Ingason et al., 2014). Thus, up to the present moment, no prior study has been able to reproduce the characteristics of IDDP-1 well using a model that explicitly includes the magmatic intrusion as well as the entire groundwater system surrounding the intrusion.

The purpose of this work is to model the production characteristics of geothermal wells drilled into superhot conditions in the vicinity of a magmatic intrusion. The model is set up to represent the first-order geologic characteristics of the Krafla geothermal system, including topography, a simplified distribution of rock types, and a magmatic intrusion at ~2 km depth. Krafla is obviously well-suited for such a study due to direct confirmation of a magmatic intrusion at depth, which is relatively rare. Although a full natural state calibration for the

Krafla system was not attempted, the model reproduces the major characteristics of the thermal structure of Krafla (for example, the transition between a near-isothermal liquid reservoir overlying a deeper boiling reservoir). Rather, the focus of this study is to calibrate the permeability structure around a well drilled into the near-vicinity of the magma intrusion to the observed discharge behavior of the IDDP-1 well (Ingason et al., 2014). Notably, this is one of the first attempts to develop a field-scale model of a geothermal system that explicitly includes a magmatic intrusion in the model domain.

2. METHODOLOGY

This study uses Complex Systems Modelling Platform (CSMP++; Matthäi et al., 2007), which incorporates a numerical scheme based on the Control Volume Finite Element method (CVFEM). Weis et al. (2014) describe in detail the numerical approach and present benchmarks of the code against other simulation platforms including TOUGH2 (Pruess et al., 1999) and HYDROTHERM (Hayba and Ingebritsen, 1997). The CVFEM approach in CSMP++ is tailored to ensure stable solutions in the presence of strong gradients in fluid properties and large fluid source terms (Weis et al., 2014), as inevitably arise in scenarios with production or injection wells at superhot/supercritical conditions. In addition, CSMP++ allows for embedded lower dimensional elements, where fractures can be modelled as 2D planes in 3D reservoirs (Patterson et al., 2018) and wells can be represented as 1D lines in 2 and 3D models (Yapparova et al., 2022). One advantage of CSMP++ compared to TOUGH2 is the ability of CSMP++ to use unstructured meshes with variable grid refinement, while the integrated finite differences method (IFD) approach of TOUGH2 uses a structural mesh that imposes constraints on the spatial discretization. However, in both cases, as substantial grid refinement would need to be applied near a well to reproduce the steep pressure gradients in the near-vicinity of a well, such grid refinement would result in very small time steps, which in the context of the IMPES-like (implicit pressure, explicit saturation) CVFEM scheme would lead to extremely long simulation times.

Since the discretization of grid blocks in a numerical reservoir model is inevitably much coarser than the diameter of wells, representing production or injection wells in numerical reservoir simulation requires the integration of a well model. To reproduce the steep pressure gradients that develop around wells and to calculate accurate production/injection rates, these models introduce an additional ‘‘well pressure’’ variable for each block containing a well in addition to the reservoir fluid pressure. We adopt the widely-used approach of Peaceman (1978) for use with the CVFEM framework within CSMP++, as described in detail in Yapparova et al. (2022), who also benchmarked the CSMP++ implementation of the Peaceman (1978) model against analytical solutions for production/injection wells as well as TOUGH2.

As the numerical method (Weis et al., 2014) and well model (Yapparova et al., 2022, 2023) have been described in detail in these previous publications and benchmarked, this section will very briefly review the numerical approach and instead focus on a description of the model set-up and main assumptions as relevant to this study.

2.1 Numerical approach

The governing equations of multi-phase mass and energy conservation are solved using a continuum porous media approach with a pressure-enthalpy-salinity-based formulation. Phase velocities are obtained using Darcy’s law. Energy conservation accounts for conduction of heat in the rock and advection of enthalpy by fluid. Source/sink terms calculated using the Peaceman (1978) model are used to represent for the energy or mass added or removed through the well fluids. Fluid and rock are assumed to be in local thermal equilibrium, and total enthalpy is distributed over fluid and rock contained in a control volume such that they are at the same temperature (Weis et al., 2014).

The model uses the Driesner (2007) and Driesner and Heinrich (2007) EoS for the H_2O–NaCl fluid system, which is valid in the temperature and pressure range from 0 to 1000 ◦C and 0 to 5000 bar. Since the fluid in this study is assumed to be pure water, and the properties in the pure H_2O limit are taken from the IAPWS-84 equation of state (Haar et al. 1984), fluid properties used in this model are derived from IAPWS-84. The reason for using this implementation compared to later IAPWS implementations is reduced computational costs; variability in fluid properties at near-critical conditions is minor (Driesner and Heinrich, 2007). In this study, we use a linear relative permeability model (X-curves) with a residual saturation of 0.3 for the liquid phase and 0.0 for the vapor phase, with $k_{r,l} + k_{r,v} = 1$. Note, however, any relative permeability model can be applied within the presented scheme if so desired.

2.2 Model set-up

The model setup aims to be broadly representative of the Krafla geothermal system and the conditions encountered in the IDDP-1 well. The 3D modelling domain is ~5 km (depending on topography) in vertical dimensions and 15 km^2 in horizontal dimensions, with the center of the model domain corresponding to the location of the IDDP-1 wellhead (Figures 3 and 4). An initial conductive heat flux of 150 mW m^{-2} results in an initial geothermal gradient of 75 °C km^{-1}. The initial pressure distribution is hydrostatic, and all boundaries are open to flow, with pressure and temperature fixed at ambient conditions (1 atm, 10 °C) at the top boundary and at hydrostatic conditions on the side boundaries.

A sill-shaped magmatic intrusion, 1 km thick and of a horizontal diameter of 4 km, is instantaneously emplaced into the host rock with a top depth of 2 km depth. The intrusion is initially at 950 °C, consistent with petrological estimates of the temperature of rhyolitic magma. The intrusion cools via conductive heat transfer across the brittle–ductile transition (BDT) to the convecting hydrothermal system in the surrounding host rock. We simulate the full evolution of the geothermal system from the incipient stage soon after the initial magma emplacement, passing through the main stage, when a high temperature geothermal system reaches close to the surface, through the waning stage, when high temperatures remains close to the surface but the intrusion is cooled at depth (Scott et al., 2016). In our production simulations, we assume that the system has reached the main stage. The amount of time required to reach the main stage mainly depends on the permeability of the basement intrusions surrounding the intrusion.

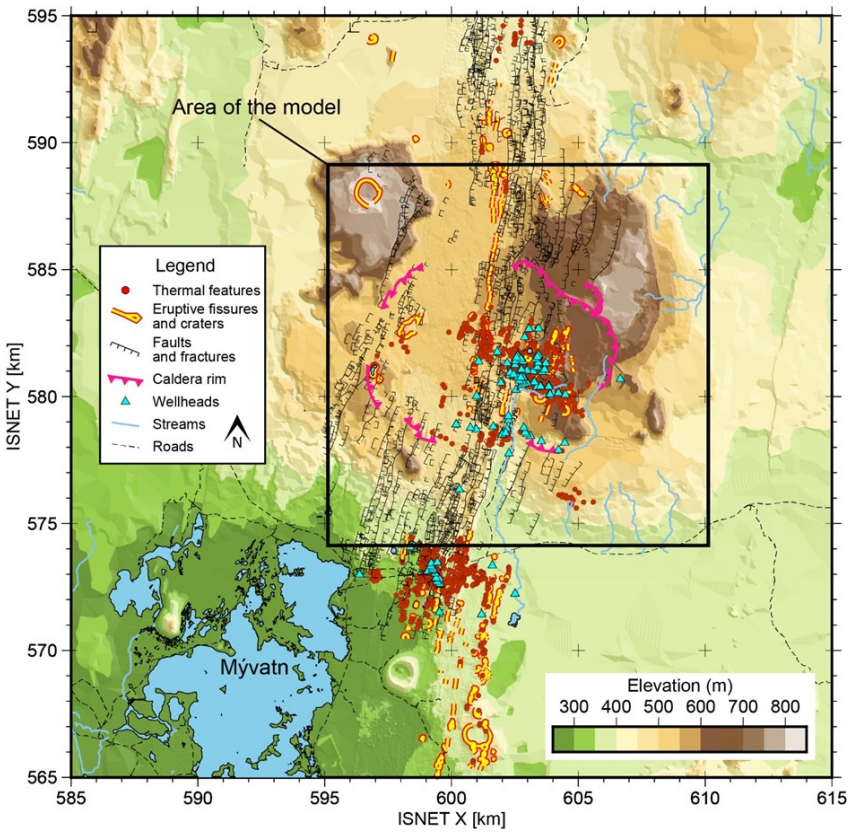

Figure 3: Map of the Krafla area showing topography as well as various geological features. The area of the model developed in this study is represented by the thick black box.

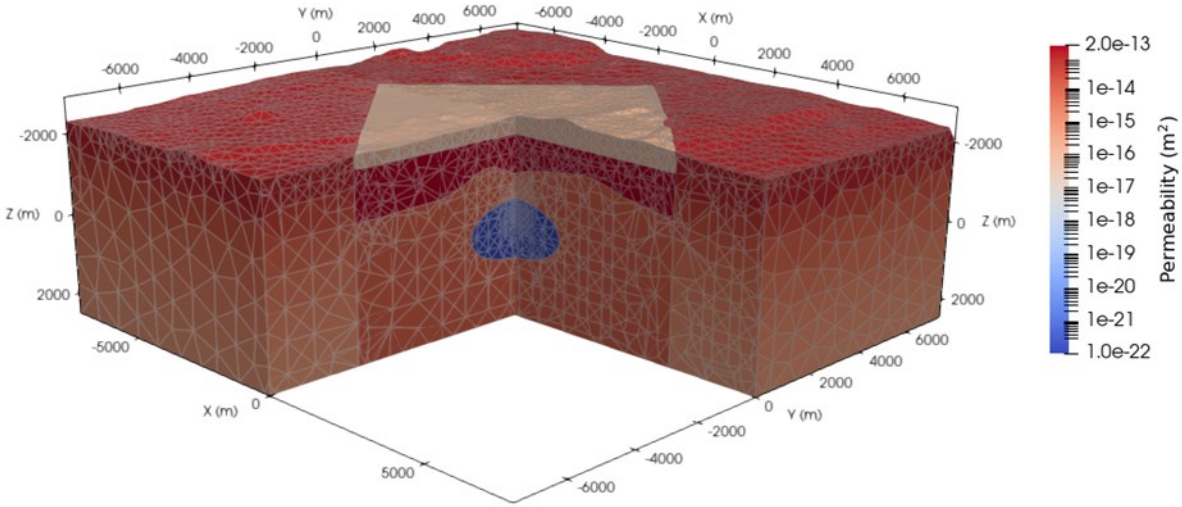

Figure 4: Finite element discretization and permeability structure of the model at the beginning of simulation time. Perspective is looking towards the northwest.

In the model, I used a simplified representation of the distribution of subsurface lithologies in the area close to the center of the caldera as shown in Figure 4. Specifically, the model includes a transition between upper high permeability volcanic rocks (hyaloclastites and lava flows) and lower permeability basement intrusions, based on previous geological investigations (Mortensen et al., 2015; Weisenberger et al., 2015). Thus, the subsurface geology is not represented in as much complexity as in a previous TOUGH-based model of Krafla (Scott et al., 2023. In addition, the previous TOUGH-based model developed by Scott et al. (2023) included a low permeability "aquiclude" (a stratigraphic unit with low permeability of ~10^{-16} m^2) at the transition between boiling conditions in the deeper basement intrusions and the near-isothermal liquid conditions in the higher permeability volcanic rocks, consistent with earlier conceptual models of the area (Böðvarsson et al., 1984). Calibration of the TOUGH model suggested that it was very difficult, if not impossible, to reproduce the

distribution of temperature and boiling conditions without including this aquiclude in the model. However, in this study, this aquiclude was not incorporated into the model, this model reproduces the isothermal character of the upper boiling zone without this aquiclude. This potentially reflects the advantage of including the full convective groundwater system and the magma-hydrothermal interface in the numerical model, rather than representing the heat source in terms of fixed boundary conditions.

Furthermore, in the TOUGH model, model calibration indicated significant permeability anisotropy. In this study, permeability was assumed to isotropic to reduce the parameter space for model calibration, given the relatively short duration of the project. Note that including permeability anisotropy is possible using CSMP++ and could be incorporated in the future. Calibration of this model indicated that the near-isothermal character of the system between ~0.5-1 km depth required a permeability of ~10^{-13} m^2. Along with the permeability of the "damage zone" around the feedzone (see below), the permeability of the basement intrusions is the main uncertain parameter in this model, and was varied between 10^{-15} – 10^{-14} m^2, consistent with estimates of the bulk permeability of this system at depths of > 1 km (Björnsson and Bödvarsson, 1990; Scott et al., 2023). A low permeability clay cap with a permeability of 10^{-16} m^2 is assumed to be present in the center of the model domain and is present in the upper ~300-400 m of the system, depending on topography. Other rock properties are assumed to be broadly representative of basalt, including porosity of 0.1, density of 2700 kg m^{-3}, and thermal conductivity of 2 W m^{-1} °K^{-1}. These properties could also be varied between different rock types (and calibrated assuming sufficient data is available) but were kept constant for simplicity. To mimic the reduction in differential stress at high temperatures and the closure of brittle fractures across the BDT, permeability is temperature-dependent (Hayba and Ingebritsen, 1997; Scott et al., 2016). As is appropriate for basaltic host rocks, the onset of the BDT occurs at 550 °C (Violay et al., 2012), above which temperature the logarithm of the permeability decreases linearly to a minimum of 10^{-22} m^2 at 700 °C.

Production is modeled using a vertical well completion interval consisting of evenly spaced well nodes (spaced 10 m) in the middle of model domain, which are initially placed inside the impermeable intrusion and become part of permeable rock as the intrusion cools. Consistent with the evidence from IDDP-1 that indicated a transition over zones of 10s-100 of m between relatively impermeable basement rock, high permeability rock close to the magma, and magma, we only model production from the nodes that are closest to the impermeable intrusion; production from the other nodes in the well completion interval is not considered. As calibration tests indicated that bulk basement permeability in the range of 10^{-15} – 10^{-14} m^2, was not consistent with the observed mass flow rates of up to ~50 kg s^{-1}, a "damage zone" with higher permeability was introduced in the vicinity of the well. The size of the damage zone was varied in a series of tests, which indicated that model calibration could be achieved if the damage zone has a diameter of around 200 m.

3. RESULTS AND DISCUSSION

The results are presented in two parts, the first concerning the "natural state" calibration and the second concerning the calibration of production behavior from an IDDP-1-like resource. As noted above, the goal in this study was not to achieve a perfect natural state calibration for the entire Krafla geothermal system, considering the measured temperatures in all drilled wells, but rather to prove that the model can represent first-order characteristics of the field, such as the transition between the shallower liquid-dominated zone and deeper boiling zone. In addition, while the calibration to the production characteristics of IDDP-1 is considered reasonably well-achieved, many questions remain as the calibration suggested by this current model is non-unique. Alternative scenarios will be considered in future versions of the model. Similarly, other improvements to the model, such as an improved representation of the size and characteristics of the intrusion and a different model for permeability evolution at BDT conditions will be implemented.

3.1 Natural state

As noted above, these models simulate the full evolution of the geothermal system, from the incipient stage soon after the initial magma emplacement, to the main stage, when a high temperature geothermal system reaches close to the surface, through the waning stage, when high temperatures remains close to the surface but the intrusion is cooled at depth (Scott et al., 2016). This approach to modeling is in stark contrast to TOUGH-based models that assume fixed boundary conditions and can therefore achieve a steady-state (i.e. unchanging) temperature and pressure distribution by simulating the system for a million years or more. This steady-state configuration is then the basis for later production simulations. In contrast, in these simulations, the "natural state" of the system depends on the time after magma emplacement and is by its nature highly dynamic. For the purposes of this study, the "natural state" of the system – i.e. the time at which production from the near-magma environment commences – occurs during the main stage, when the thermal anomaly introduced by the cooling magma reaches close to the surface. Because the rock permeability close to the intrusion controls the velocity of groundwater convection and the cooling behavior of the magma, this time differed for the different simulations, ranging from ~400 years for simulations with high basement permeability (10^{-14} m^2) to ~1500 years for simulations with intermediate basement permeability (10^{-15} m^2).

Figure 5 shows a series of 2D cross-sections through the center of the 3D model, showing the thermal structure of different systems as a function of the permeability of the basement intrusions between 10^{-15} and 10^{-14} m^2. In these figures, the transitions between the "rock types" (i.e. from basement intrusions to high permeability upper volcanics, and from upper volcanics to the low permeability clay cap) are represented by dashed lines. The red lines show temperature isotherms, the blue lines pressure isobars, and colors show the vapor saturation, and white areas correspond to zones of single-phase liquid. The grey color shows the area of the intrusion, defined by having a permeability <10^{-16} m^2. From Figure 5, it is clear that lithological transitions cause significant variability in the thermal structure, with boiling zones with higher vapor saturations confined to the deeper basement intrusions. Whether boiling conditions extend to shallower depths depends on the permeability of the basement intrusions. If permeability is 10^{-15} m^2 (Fig. 5a), boiling conditions are confined to the basement intrusions. If permeability is 5 x 10^{-15} m^2 (Fig. 5b), there is a small boiling zone towards the top of the upper volcanics, near the boundary with the clay cap. If permeability if 10^{-14} m^2 (Fig. 5c), boiling conditions are present throughout much of the upflow above the basement intrusions. In all cases, zones of single-phase vapor (vapor saturation = 1) are present close to the intrusion. These zones tend to be larger if rock permeability is lower.

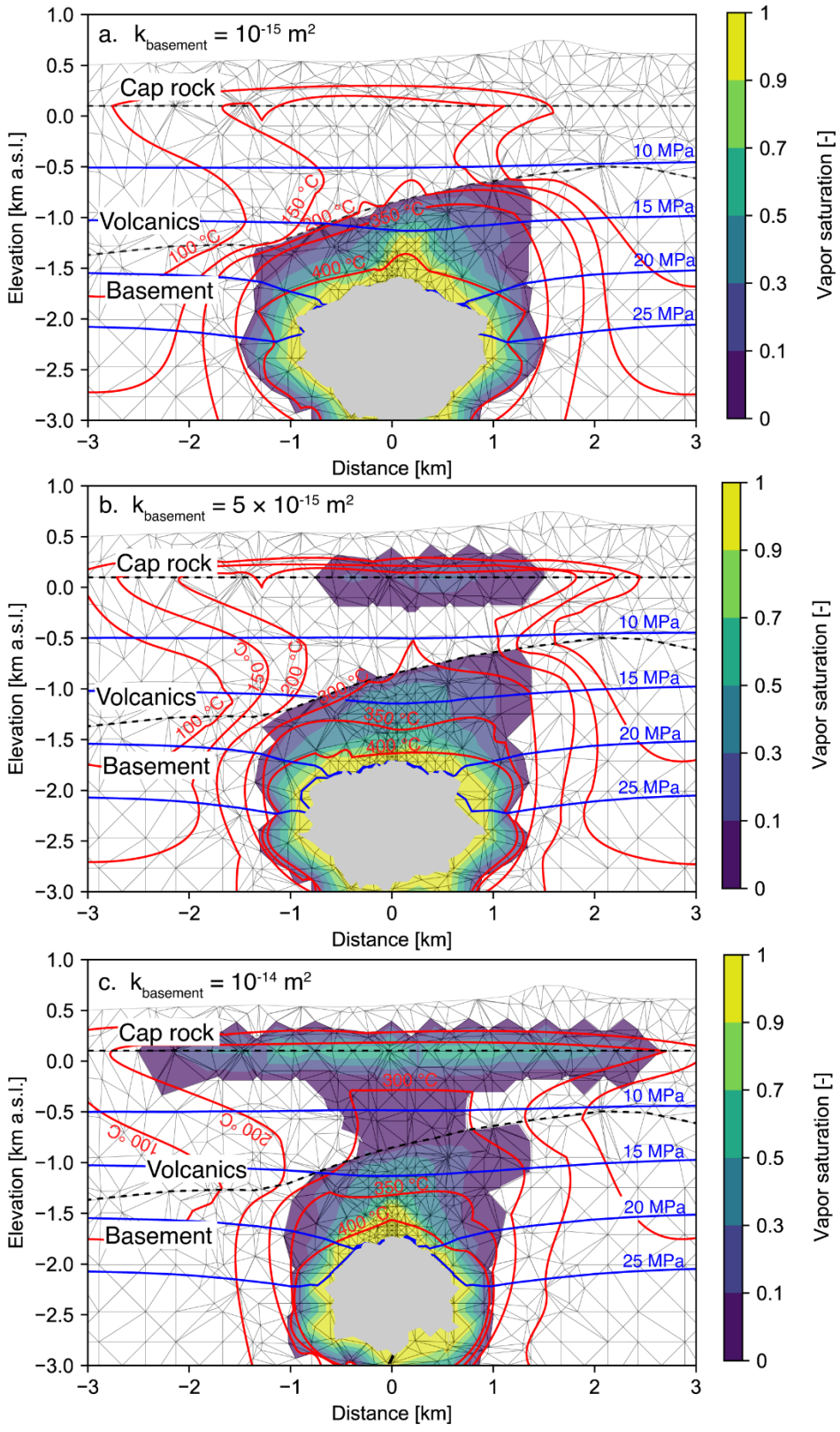

Figure 5: 2D cross-sections through the center of the model domain, showing the thermal structure and vapor saturation (colors) of different systems with basement permeability ($k_{basement}$) of a. 10^{-15} m², b. 5 x 10^{-15} m² , or c. 10^{-14} m² . Transitions between the rock types represented by dashed lines. Red lines show temperature isotherms, the blue lines pressure isobars, and white areas correspond to zones of single-phase liquid. The grey color shows the area of the intrusion, defined by having a permeability <10^{-16} m².

From the temperature isotherms in Figure 5, it is also clear that higher permeability in the basement intrusions leads to higher temperatures in the upper volcanics. While achieving a perfect calibration to Krafla wells was not an objective of this study due to limited time, one goal of this work was to try to reproduce the isothermal character of the shallow liquid-only zone, as well as its approximate temperature. Figure 6 compares modeled temperature-depth relations colored lines with measured temperature-depth profiles in IDDP-1 (black dashed line) as well as other wells in the Leirbotnar/Vítismór subfields (grey lines). The different lines represent different models with basement permeability between 10^{-15} and 10^{-14} m^2. The permeability of upper volcanics was set to a value of 2×10^{-13} m^2, based on tests indicating that this was the minimum permeability needed to achieve a near-isothermal character over the entire upper volcanics.

There are a couple features evident from Figure 6 that reveal both discrepancies and similarities to the measured thermal structure of the Krafla geothermal system. First, the clay cap thickness assumed in the models is clearly too large. This causes the linear conductive temperature profiles to extend for too large of a depth range, and the temperatures at the surface to be too low. If there was additional time to re-run these models in the interest of achieving a better "natural state" calibration, this would be one of the first features to be changed. In addition to this discrepancy, Figure 6 shows that temperatures in the isothermal zone for IDDP-1 are somewhat lower (180 °C) than the lowest modeled temperature in the isothermal zone (~200 °C), which results when basement permeability is 10^{-15} m^2. However, this figure also shows that IDDP-1 is an outlier compared to other nearby wells by having these lower formation temperatures. One possibility is that IDDP-1 had not finished heating up by the time the measurement shown on Figure 6 was performed (216 days after heating; data is from Mortensen et al., 2014). With that in mind, comparison of the model results with the measurements suggests that simulations with a basement permeability of ~10^{-15} to ~2.5×10^{-15} m^2 (likely a bit higher) are broadly consistent with the isothermal zone temperatures in Leirbotnar and Vítismór.

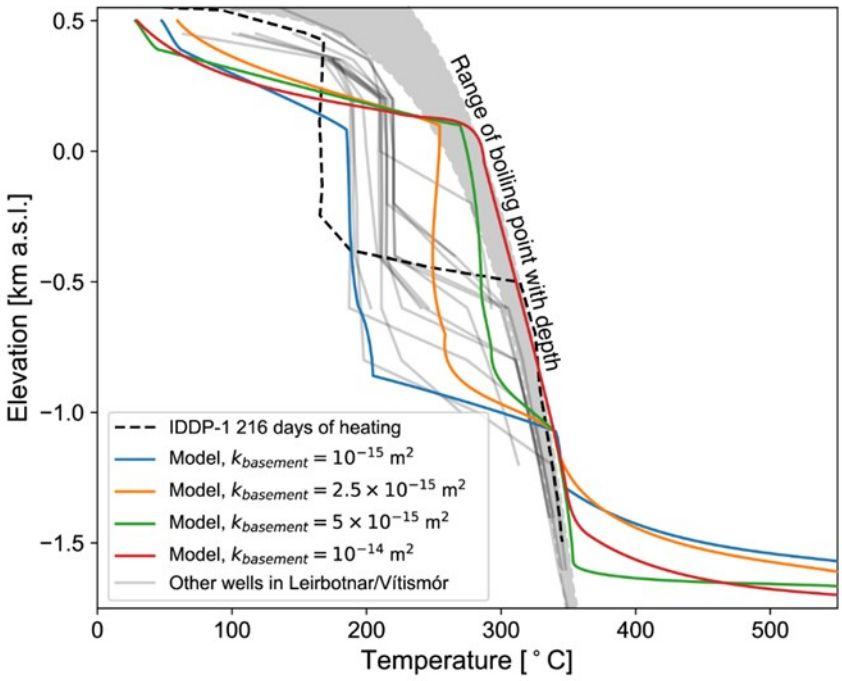

Figure 6: Comparison of modeled temperature-depth relationships in the center of the model with measurements from IDDP-1 (black dashed line) and other wells in Leirbotnar/Vítismór. The grey area shows the range of boiling point with depth, depending on the elevation of the water table, which is variable in the model.

As noted above, one feature of this model that differs significantly from the TOUGH-based model of Scott et al. (2023) is that a low permeability aquiclude at the transition between the basement intrusions and upper volcanics was not included. In the TOUGH model, the thickness of this layer could be adjusted so as to match the thickness of the isothermal zone. As it was not included in the model in this study, there are some discrepancies in the thickness of the isothermal zone between the model and the data. In particular, it appears that the transition to the basement intrusions is occurring too deeply in the model, as evidenced by the much thinner isothermal zone in the IDDP-1 data compared to the models. However, there is also significant variability throughout the Leirbotnar subfield. This likely reflects the fact that the "basement intrusions" lithologic transition is only approximately defined (more of a statistical transition where the bedrock is increasingly comprised of intrusions, rather than a stratigraphic transition). Perhaps one useful revision to the model that would improve the "natural state" fit would involve changing the depth to the basement intrusions based on the measured temperature profiles; however, this would inevitably result in some discrepancies compared to the original geologic model (Weisenberger et al., 2015) used as the foundation for the TOUGH model as well as this study.

3.2 Production modeling from superhot resources

In standard approaches to geothermal reservoir modeling, following calibration of the 'natural state' temperature distribution, the next step is to further refine the model calibration using production data such as discharge enthalpy, mass flow rate, and temperature/pressure changes. While this study focuses exclusively on simulating production from the superhot environment (IDDP-1-like conditions), it is still useful to compare the range of well discharge enthalpies encountered in the Krafla field with the simulated "natural state" enthalpy distribution in these models. Figure 7 compares measured discharge enthalpies (using data from Hermanska et al., 2014) and inferred reservoir pressures for production wells in Krafla with the simulated pressure-enthalpy distribution along the main axis of the upflow in the simulations. While some "liquid" enthalpy wells match the approximate range of p-H relations for systems with basement permeability ~10^{-15} to ~2.5×10^{-15} m^2, most of the wells can be classified as 'excess enthalpy' wells, with discharge enthalpies significantly in excess of the initial reservoir fluid enthalpy. These wells are believed to result from boiling processes in the reservoir around the production well that cause vapor to be enriched in the two-phase fluid that flows towards the well, and liquid to be retained in the aquifer – this process is known as phase segregation (Arnorsson et al., 1990; Scott et al., 2014). Most studies up to the present moment have focused on accounting for phase segregation in terms of fluid chemistry, so that initial aquifer fluid compositions can be reconstructed from chemical analysis of liquid and vapor sampled at the surface (Gudmundsson and Arnorsson, 2002; Karingithi et al., 2010; Scott et al., 2014). However, the physics of this process remain generally understudied. In addition to phase segregation, Figure 7 suggests that several of the 'acid' wells (open symbols in Fig. 7) might result from addition of deep superhot vapor to the well discharge..

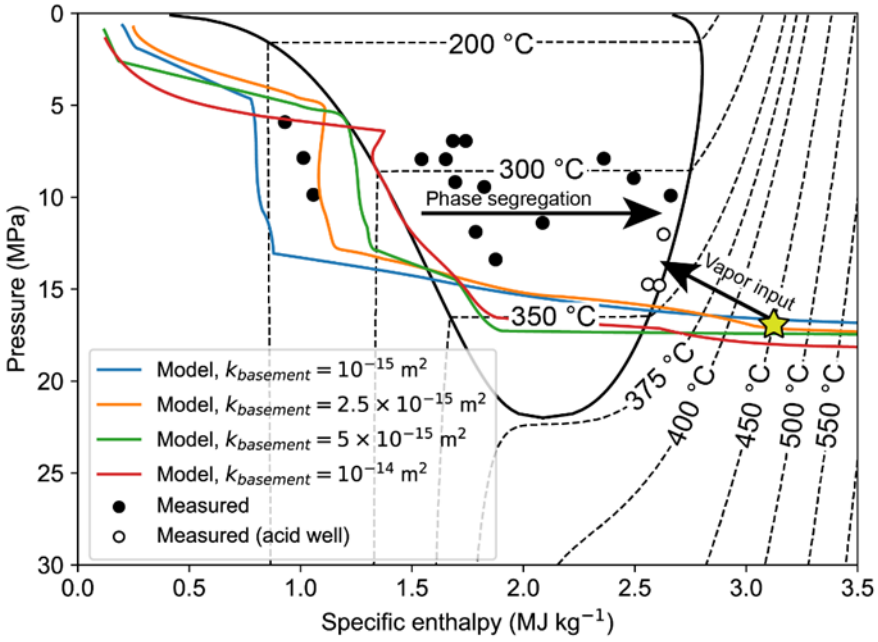

Figure 7: Comparison of discharge enthalpy of Krafla wells (circles) with simulated enthalpy distribution along the upflow zones of the simulations, for different values of basement permeability. The measured conditions of the IDDP-1 reservoir are represented by the star.

Instead of attempting to match the range of production characteristics across the Krafla system, the focus of this study is on production from the superhot environment, and particularly how production characteristics depend on reservoir permeability. The results show that the characteristics – both discharge enthalpy and mass flow – are highly dependent on reservoir permeability structure. Similar to Figure 5, Figure 8 shows a series of 2D cross-sections through the center of the 3D model, showing the enthalpy, temperature and fluid pressure distribution near the intrusion of different systems as a function of the permeability of the basement intrusions between 10^{-15} and 10^{-14} m^2. The permeability of the damage zone is 10^{-13} m^2 in all simulations in Fig. 8, which shows properties after 1 day of production. The stars represent the nodes that were simulated as the production interval. These nodes were selected based on a temperature-criterion – since the brittle-ductile transition was assumed to occur at 550 °C, and evidence from the drilling of IDDP-1 suggests that most of the inflow into the well occurred very close (within 10s of m) of the magma, the nodes that were closest to 550 °C without exceeding 550 °C were selected as the production nodes. These nodes were assigned a flowing bottom-hole pressure of 10 MPa, which is less than the initial reservoir pressure at these depths of ~18 MPa.

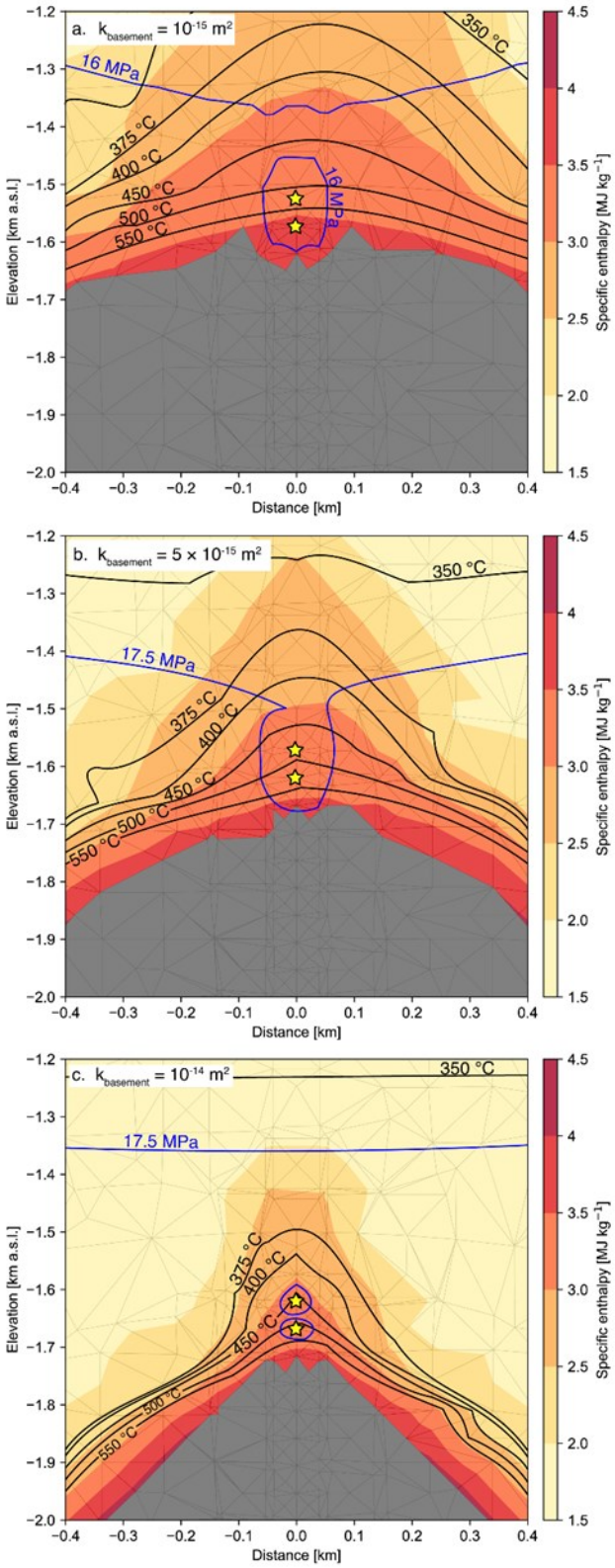

Figure 8: 2D cross-sections through the center of the model domain, showing the thermal structure and specific enthalpy (colors) of different systems with basement permeability ($k_{basement}$) of a. 10^{-15} m², b. 5 x 10^{-15} m² , or c. 10^{-14} m² . Black lines show temperature isotherms, the blue lines pressure isobars, and the grey color shows the area of the intrusion, defined by having a permeability <10^{-16} m². The stars represent the production nodes (see text).

Figure 8 shows that temperature and enthalpy vary rapidly close to the intrusion, but generally both temperature and enthalpy increases with decreasing host rock permeability, as shown schematically in Figure 2. For a system with basement permeability of 10^{-15} m^2 (Fig. 8a), zones with temperatures >400 °C and fluid enthalpy exceeding 3 MJ kg^{-1} extend upwards to ~-1.4 km a.s.l. For a system with basement permeability of 5×10^{-15} m^2 (Fig. 8b), such zones extend upwards to ~-1.5 km a.s.l. Temperature and enthalpy gradients are particularly tight in a system with host rock permeability of 10^{-14} m^2 (Fig. 8c). Fluid enthalpy increases from ~2 to ~3 MJ kg^{-1} and temperature increases from 375 to 550 °C over a distance of 100-200 m. Although the temperature distribution close to the magma chamber is highly uncertain, the latter characteristics appear to be more consistent with the experience of IDDP-1 and the steep transition from boiling point with depth conditions to magma.

Although Figure 8 shows the fluid pressure distribution after only 1 day of production, the basement permeability clearly exerts a major control on the impact fluid extraction has on the size of the depressurization zone surrounding the wellbore. This is because fluid can recharge the production zone less efficiently if basement permeability is lower. However, the zone of particularly low fluid pressures approximately corresponds to the damage zone, as shown clearly in Fig. 7a and 7b. Due to the relatively higher permeability of the damage zone, most of the produced fluid is derived from the damage zone. The greater the permeability contrast between the damage zone and the surrounding basement, the greater the fluid pressure difference between the damage zone and the surrounding basement. As a result, this resulted in very rapid depressurization of the damage zone for simulations with basement permeability of 10^{-15} m^2. Within timescales of a few days/weeks, reservoir pressure would fall beneath the flowing bottom-hole pressure of 10 MPa, even though mass flow rates from these wells were relatively low. This indicates that the size of the damage zone needs to be large enough to account for the measured discharge rates, or that the permeability of the basement needs to be high enough so that the contrast between the damage zone and the surrounding basement is not so extreme.

This dynamic can be seen in Figure 9, which plots the average reservoir fluid pressure at the two production nodes and mass flow rate from the production well for simulations with low basement permeability of 10^{-15} m^2 and damage zone permeability of 10^{-14} – 10^{-13} m^2. For a simulation with a damage zone permeability, 10^{-14} m^2, production rates are low (~4 kg s^{-1}). For the simulations with damage zone permeability of 5 x 10^{-14} m^2 or 10^{-13} m^2, the production rates at the onset of production are 10-15 kg s^{-1}, but reservoir fluid pressure reaches the flowing bottomhole pressure after only a few days. This leads to the termination of production in the simulation, since at that point the production nodes turn into injection nodes since the well pressure at these nodes is greater than the reservoir pressure, i.e., fluid would leave the wellbore and go into the formation. In addition to the relatively low mass flow rates, the temperature and enthalpy at the production zone are too high (~550 °C and 3.4 MJ kg^{-1}), which is significantly higher than observed in the IDDP-1. This suggests that this set of conditions (basement permeability of 10^{-15} m^2) does not reproduce the characteristics of the IDDP-1 discharge very well.

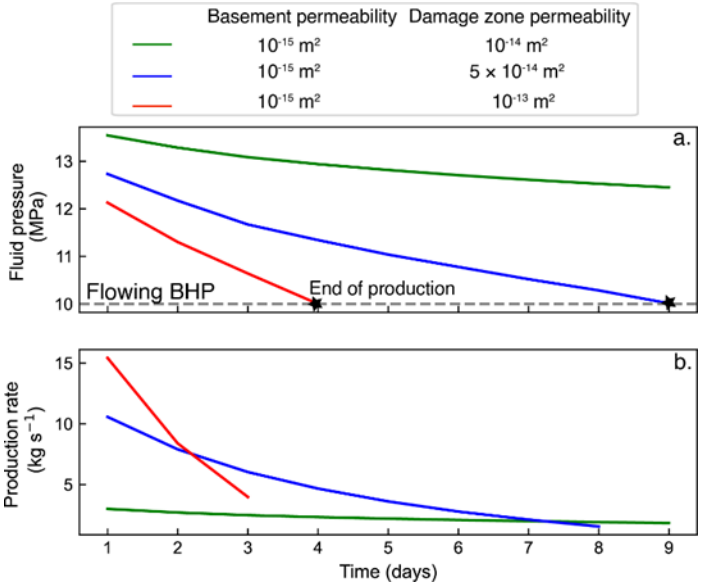

Figure 9: Evolution of (a) fluid pressure and (b) production rate over the first 9 days of production for simulations with low basement permeability (10^{-15} m^2) and damage zone permeability of 10^{-14} – 10^{-13} m^2.

Figure 10 shows results for simulations with high basement permeability of 10^{-14} m^2 and damage zone permeability of 10^{-14} – 10^{-13} m^2, additionally superimposing the measurements from the discharge tests of IDDP-1 in the spring/summer of 2011. High basement permeability combined with damage zone permeability of 5×10^{-14} – 10^{-13} m^2 appears to match the IDDP-1 results of all the conditions considered in this study, reproducing the range of measured wellhead temperatures, discharge enthalpies, and production rates. However, these simulations additionally show a relatively rapid rate of temperature, pressure and enthalpy decrease, which is most rapid for the high damage zone permeability (10^{-13} m^2). Enthalpies decrease to <3 MJ kg-1 after ~50 days of production. After ~150 days of production, there is a sudden shift decrease in discharge enthalpy as the superhot conditions shift to two-phase conditions, leading to a significant decline in the thermal output of the well from ~120 MWth to <100 MWth.

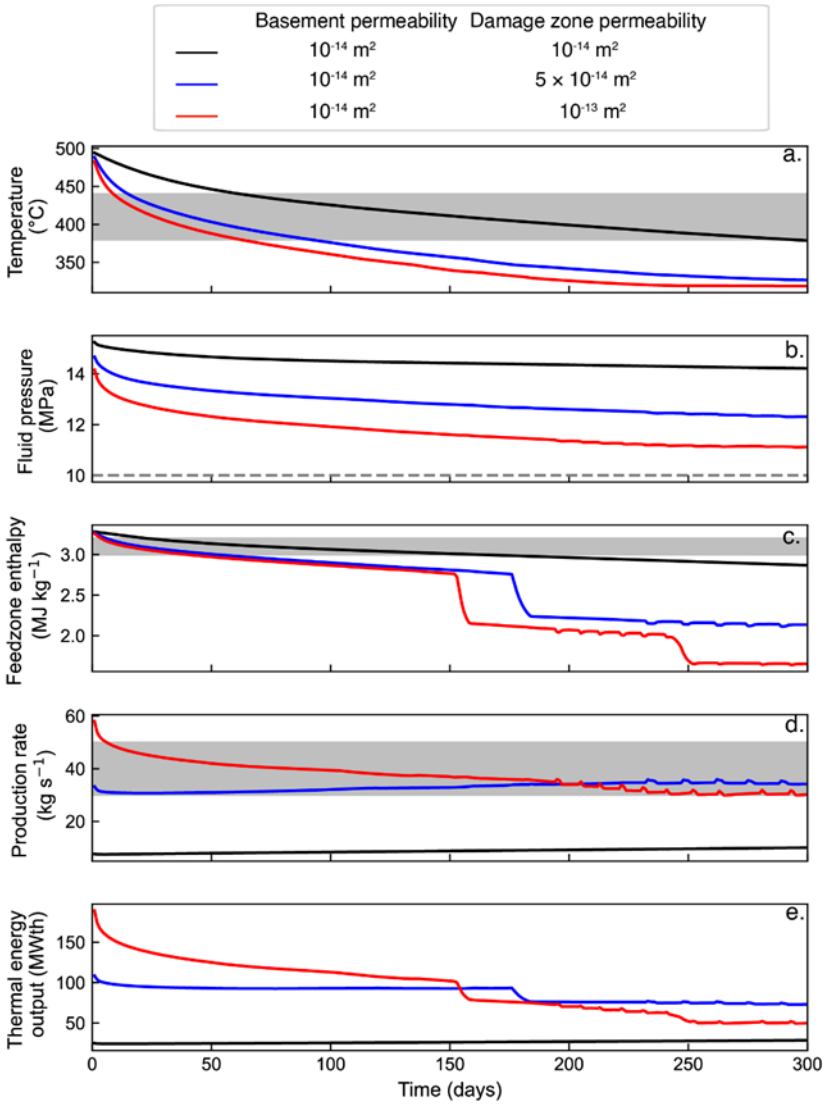

Figure 10: Evolution of (a) temperature, (b) fluid pressure, (c) enthalpy, (d) production rate and (e) thermal energy output over the first 9 days of production for simulations with high basement permeability (10^{-14} m^2) and damage zone permeability of 10^{-14} – 10^{-13} m^2.

The rapid decrease in temperature and enthalpy is attributed to the influx of cooler circulating waters from the surrounding basement towards the production well. As can be seen in Fig. 8c, the size of the zone with superhot temperatures only extends ~100 m from the production nodes. As the depressurization zone around the well draws these cooler waters towards the production well, the magmatic heat source is unable to heat these fluids to superhot conditions prior to their being produced by the well.

These results highlight the potential for decreasing enthalpies due to the process of colder water recharge. However, it should be noted that these results are a consequence of the assumptions embedded in the models. These include: (i) the permeability structure of the basement rock and damage zone, and (ii) the geometry of the intrusion at the onset of production. If the intrusion was 'flatter' at the top and the damage zone from which the production well draws fluid extended around the perimeter of the intrusion (corresponding to an intensely fractured zone at the contact zone of the intrusion with the surrounding host rock), we would likely not observe these results. However, investigating these scenarios would require more time and additional model set-ups considering alternative models for near-magma permeability structure and intrusion geometry.

Although our model is able to roughly match the production characteristics of the IDDP-1 well, it does not match the exact transient fluctuations observed in the flow tests. This could result from our assumption of a constant bottomhole flowing pressure, whereas well head pressure during the flow tests was more variable. Moreover, we did not simulate a stage of cold-water injection during drilling, there is no heating up stage of the well in our models. Lastly, our model simplifies the complex geologic structure around the rhyolitic magma chamber beneath Krafla; much remains to be explored both geologically and by using computer models. This work is beyond the scope of this current study but will be investigated in more detail in the future.

4. CONCLUSIONS AND NEXT STEPS

A "first of its kind" geothermal reservoir model explicitly including a magmatic heat source has been developed for the Krafla system. Despite simplifying assumptions related to the subsurface geology, this model can roughly reproduce the range of measured temperatures in Krafla. The contrast between the boiling point with depth conditions in Suðurhlíðar and the shallow isothermal liquid zone in Leirbotnar likely result from contrasts in basement permeability, with the former corresponding to higher basement permeability likely related to the Hveragil eruptive fissure. The model best able to match the approximate range of discharge characteristics in IDDP-1 features high basement permeability (10^{-14} m^2) and a damage zone permeability of 10^{-13} m^2. Although these conditions lead to a rapid decline in well discharge enthalpy, this result is likely a consequence of our model assumptions, in particular the near-magma permeability structure and the geometry of the intrusion. Better constraints on these assumptions would improve the model results.

Future work should additionally seek to better constrain the rate of heat transfer across the magma chamber. Currently, our model is predicting a lower thermal gradient across the magma-hydrothermal boundary than observed (Figure 11). Currently, the conductive heat fluxes ($Q = \lambda \times \Delta T/dz$) across the magma-hydrothermal boundary are almost an order of magnitude less than the IDDP-1 values. According to figure 1, the measured $\Delta T/dz$ is ~16 °C m^{-1}, corresponding to a conductive heat flux of ~24 W m^{-2} assuming thermal conductivity λ equal to 1.5 W m^{-1} K^{-1} (Eichelberger, 2020). In contrast, the modeled $\Delta T/dz$ is ~2 °C m^{-1}, corresponding to a heat flux of ~4 W m^{-2}, as our model assumes a constant thermal conductivity 2 W m^{-1} K^{-1}. This discrepancy could also potentially account for the rapid decrease in production enthalpy observed in Figure 10.

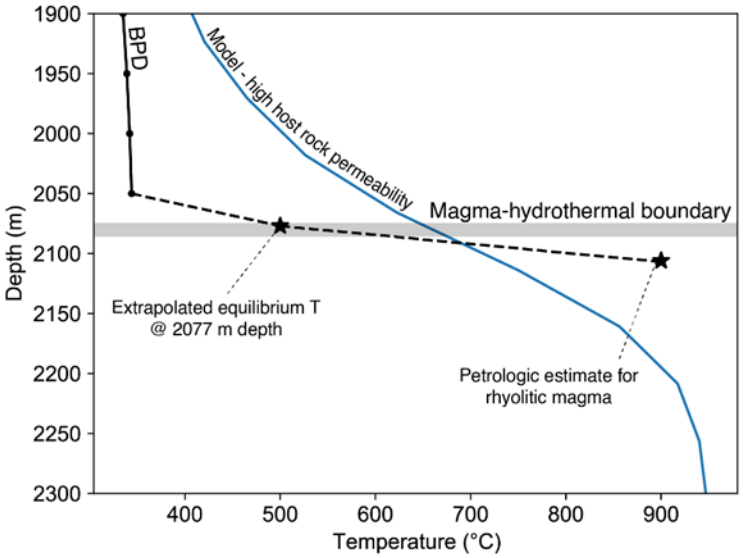

Figure 11: Comparison of modeled and measured temperature profiles across the magma-hydrothermal interface at the base of IDDP-1 (Eichelberger, 2020). The blue line shows model results assuming high basement permeability (10^{-14} m^2).

Currently, there are two main strategies for improving the fit observed in Figure 11. The first involves increasing the permeability of the damage zone or the size of the damage zone, potentially so that it envelops the intrusion. Higher rates of advective heat transport would correspond to higher rates of conductive heat transport from the intrusion, thus increasing the temperature gradient. However, this could potentially require developing a new constitutive model for permeability (i.e., going beyond the currently assumed smooth decrease in permeability above a temperature of 550 °C). Further it may require higher grid resolution, which would increase computational expense. In general, however, this would be feasible to implement in CSMP++. The second strategy to improve the fit would be to implement magma convection, which would also accelerate heat transport from the magma, likely leading to higher temperature gradients across the BDT. Magma convection is likely given the temperature and viscosity of the rhyolitic magma in Krafla (Eichelberger, 2020). This is also possible and has been implemented in other studies using CSMP++ (Andersen and Weis, 2020).

REFERENCES

Albertsson, A., Bjarnason, J. Ö., and Gunnarsson, T.: IDDP Feasibility Report Part 3: Fluid Handling and Evaluation. (2003).

Andersen, C., and Weis, P.: Heat transfer from convecting magma reservoirs to hydrothermal fluid flow systems constrained by coupled numerical modelling. Geophys. Res. Lett., 47, (2020), e2020GL089463.

Axelsson, G., Egilson, T., and Gylfadóttir, S.: Modelling of Temperature Conditions Near the Bottom of Well IDDP-1 in Krafla, Northeast Iceland, Geothermics, 49, (2014), 49–57.

Battistelli, A., Finsterle, S., Marcolini, M., and Pan, L.: Modeling of Coupled Wellbore-Reservoir Flow in Steam-Like Supercritical Geothermal Systems, Geothermics, 86, (2020), 101793.

Björnsson, G. and Bödvarsson, G.: A Survey of Geothermal Reservoir Properties, Geothermics, 19, (1990), 17–27.

Bödvarsson, G., Pruess, K., Stefánsson, V., and Eliasson, E.T.: The Krafla Geothermal Field, Iceland 2. The Natural State of the System. Water Resources Research, 20, (1984), 1531–1544.

Croucher, A.E., and O'Sullivan, M.J.: Application of the Computer Code TOUGH2 to the Simulation of Supercritical Conditions in Geothermal Systems, Geothermics, 37, (2008), 622–634.

Driesner, T.: The system H_2O-NaCl. Part II: Correlations for Molar Volume, Enthalpy, and Isobaric Heat Capacity from 0 to 1000 °C, 1 to 5000 bar, and 0 to 1 X_{NaCl}, Geochimica et Cosmochimica Acta, 71(20), (2007), 4902–4919.

Driesner, T., and Heinrich, C. A.: The system H_2O–NaCl. Part I: Correlation Formulae for Phase Relations in Temperature–Pressure–Composition Space from 0 to 1000°C, 0 to 5000 bar, and 0 to 1 X_{NaCl}, Geochimica et Cosmochimica Acta, 71(20), (2008), 4880–4901.

Eichelberger, J.: Distribution and Transport of Thermal Energy Within Magma–Hydrothermal Systems, Geosciences (Switzerland) 10, (2020), 1–26.

Elders, W.A., Friðleifsson, G.Ó., and Albertsson, A.: Drilling into Magma and the Implications of the Iceland Deep Drilling Project (IDDP) for High-Temperature Geothermal Systems Worldwide, Geothermics, 49, (2014), 111–118.

Friðleifsson G.Ó., Elders, W.A., and Albertsson, A.: The concept of the Iceland Deep Drilling Project, Geothermics, 49, (2014), 2–8.

Haar, L., Gallagher, J.S., Kell, G.: NBS/NRC Steam Tables, Hemisphere Publishing, Washington, (1984).

Hayba D.O., and Ingebritsen S.E.: Multiphase Groundwater Flow Near Cooling Plutons, Journal of Geophysical Research, 102, (1997), 12235–12252.

Heřmanská, M., Stefánsson, A., and Scott S.: Supercritical Fluids Around Magmatic Intrusions: IDDP-1 at Krafla, Iceland, Geothermics, 78, (2019), 101–110.

Ingason, K., Kristjánsson, V., and Einarsson, K.: Design and Development of the Discharge System of IDDP-1, Geothermics, 49, (2014), 58–65.

Ingebritsen, S.E., and Manning, C.E.: Permeability of the Continental Crust: Dynamic Variations Inferred from Seismicity and Metamorphism, Geofluids, (2010), 193–205.

Manning, C.E., and Ingebritsen, S.E.: Permeability of the Continental Crust: Implications of Geothermal Data and Metamorphic Systems, Reviews of Geophysics, 37, (1999), 127–150.

Magnusdottir, L., and Finsterle, S.: An iTOUGH2 Equation-of-State Module for Modeling Supercritical Conditions in Geothermal Reservoirs, Geothermics 57, (2015), 8–17.

Matthäi, S.K., Geiger, S., Roberts, S.G., Paluszny, A., Belayneh, M., Burri, A., Mezentsev, A., Lu, H., Coumou, D., Driesner, T., Heinrich, C.A.: Numerical Simulation of Multi-Phase Fluid Flow in Structurally Complex Reservoirs, Geol. Soc. London, Spec. Publ., 292, (2007), 405–429.

Mortensen, A., Guðmundsson, Á., Steingrímsson, B., Sigmundsson, F., Axelsson, G., Ármannsson, H., Björnsson, H., Ágústsson, K., Sæmundsson, K., Ólafsson, M., Karlsdóttir, R., Halldórsdóttir, S. and Hauksson, T. The Krafla Geothermal System: Research Summary and Conceptual model revision, Iceland Geosurvey. Reykjavik, Iceland. (2015).

O'Sullivan, M.J.O., O'Sullivan, J.P.O. Reservoir Modeling and Simulation for Geothermal Resource Characterization and Evaluation, in Geothermal Power Generation, (2016).

Patterson, J.W., Driesner, T., Matthai, S., and Tomlinson R.: Heat and Fluid Transport Induced by Convective Fluid Circulation Within a Fracture or Fault, J. Geophys. Res. Solid Earth, 123, (2018), 2658–2673.

Peaceman, D.W. Interpretation of Well-Block Pressures in Numerical Reservoir Simulation, Society of Petroleum Engineers, 6893, (1978), 183–194.

Pruess, K., Oldenburg, C., and Moridis, G.: TOUGH2 User's Guide, Version 2.0., Berkeley, California, (1999).

Reinsch, T. et al.: Utilizing supercritical geothermal systems: a review of past ventures and ongoing research activities, Geothermal Energy, 5, (2017), 16.

Rutter, E. H.: On the nomenclature of mode of failure transitions in rocks, Tectonophysics, 122, (1986), 381–387.

Scott, S., Driesner, T., and Weis, P.: Geologic controls on supercritical geothermal resources above magmatic intrusions, Nature Communications, 6, (2015), 7837.

Scott S., Driesner, T. and Weis, P.: The thermal structure and temporal evolution of high-enthalpy geothermal systems, Geothermics 62, (2016), 33–47.

Scott S., O'Sullivan, J. P., Maclaren, O. J., Nicholson, R., Covell, C., Newson, J., and Guðjónsdóttir, M. S.: Bayesian Calibration of a Natural State Geothermal Reservoir Model, Krafla, North Iceland, Water Resources Research, 58, (2022).

Weis, P., Driesner, T., Coumou, D., and Geiger, S.: Hydrothermal, multiphase convection of H_2O-NaCl fluids from ambient to magmatic temperatures: a new numerical scheme and benchmarks for code comparison, Geofluids, 14, (2014), 347–371.

Weisenberger, T. B., Axelsson, G., Arnaldsson, A., Blischke, A., Óskarsson, F., Ármannsson, H., Blanck, H., Helgadóttir, H. M., Berthet, J.-C. C., Árnason, K., Ágústsson, K., Gylfadóttir, S. S., and Guðmundsdóttir, V.: Revision of the Conceptual Model of the Krafla Geothermal System, Iceland Geosurvey, Reykjavik, Iceland, (2015).

Violay, M., Gibert, B., Mainprice, D., Evans, B., Dautria, J.-M., Azais, P., and Pezard, P.: An experimental study of the brittle-ductile transition of basalt at oceanic crust pressure and temperature conditions, J. Geophys. Res. Solid Earth, 117, (2012).

Yapparova, A., Lamy-Chappuis, B., Scott, S. W. and Driesner, T.: A Peaceman-type well model for the 3D Control Volume Finite Element Method and numerical simulations of supercritical geothermal resource utilization, Geothermics, (2022) 105, 102156.

Yapparova, A., Lamy-Chappuis, B., Scott, S. W., Gunnarsson, G., and Driesner, T.: Cold water injection near the magmatic heat source can enhance production from high-enthalpy geothermal fields, Geothermics, 112, (2023), 102744.

Yano Y., and Ishido T.: Numerical investigation of production behavior of deep geothermal reservoirs at super-critical conditions, Geothermics, 27, (1998), 705–721.